Quantifying and increasing the value of multi-azimuth seismic

Ted Manning, BP Sunbury, London, Middlesex, UK
Nick Shane, BP Internship, Sunbury, London, Middlesex, UK
Chris Page, PGS Walton, Surrey, UK
Brian Barley, Walter Rietveld, and Jim Keggin, BP Digla, Cairo, Egypt

Conventional marine exploration offshore Nile Delta is challenged by shallow heterogeneities and a deep, complex anhydrite layer called the Messinian. These subsurface complexities cause variable illumination and strong diffracted multiples resulting in imaging challenges below the anhydrite on conventional narrow-azimuth towed streamer acquisition because the recording antenna is too small (Figure 1a). Additionally, it has proved difficult to build the detailed depth migration velocity model required to correctly image below the Messinian layer. Multi-azimuth (MAZ) acquisition using time-domain processing however, has been very successful in addressing both the noise and illumination problems in the Nile Delta. The increased azimuthal and crossline offset coverage—bigger antenna—is achieved by acquiring six conventional marine surveys over the same area at 30° sail-line increments (Figure 1b).

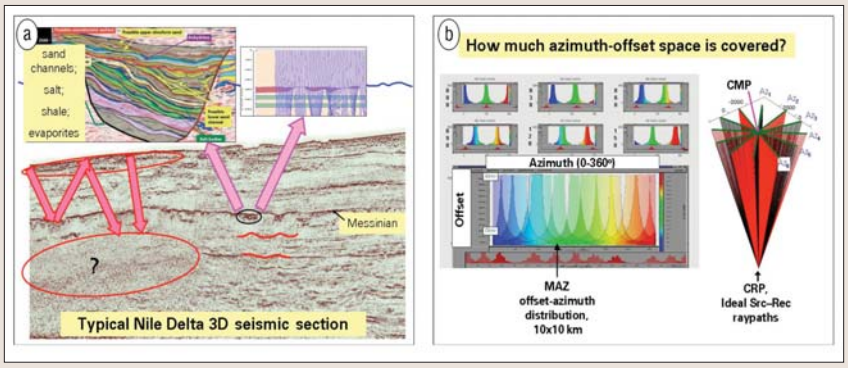

Figure 1. *(a) Nile Delta exploration challenges—note the complex water bottom, diffracted multiple problem and wavefield distortion (ray bending) effects at the Messinian layer. (b) The multi-azimuth acquisition azimuthal diversity is shown in the cartoon on the right. The azimuth and offset-space coverage is mapped out using the Raven geometry files on the left, for each of the six azimuths (top), and for the combined data set (bottom). Colors represent azimuth while the intensity respresents fold.*

The simple stack of the Raven multi-azimuth survey is robust, with increased signal-to-noise (S/N) ratio, increased spatial and temporal resolution, and increased overall image quality, resulting from the combination of the additional azimuth volumes (sectors). This paper will discuss how additional azimuths add value at Raven, and show that the simple stack of all azimuth sectors may be improved upon.

This paper is divided into three parts. Firstly, quantitative data analysis is presented to understand the success of multi-azimuth seismic at Raven. Secondly, the "quality curve" concept is used to quantify the additional value that each azimuth adds to the MAZ result. Thirdly, simply stacking the data, while robust, is shown to be suboptimal, and new processing techniques are discussed that can further improve the MAZ seismic quality during volume combination.

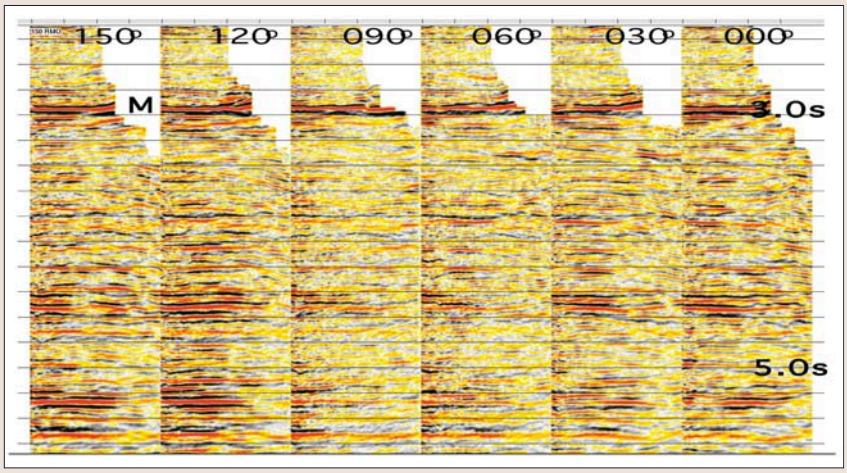

Figure 2. *3D common image point example after time migration and after independent residual moveout, from all six azimuths (ensemble median gain applied). The Messinian event is highlighted by the "M." Note the varying signal and noise characteristics with offset and azimuth.*

Background. Since gas was first discovered in the Nile Delta, most exploration programs have focused on shallow Pliocene reservoirs, where gas can clearly be seen as bright events on high-quality seismic data. The petroleum geology of the deeper pre-Pliocene section is similar to the Pliocene, where potential reservoirs consist of sand-prone channel systems originating from the Nile, yet deeper exploration had not been possible for two reasons. Firstly, deeper burial and harder rocks mean that hydrocarbons are less visible on our seismic data. Secondly, pre-Pliocene seismic quality is highly variable and often very poor (Figure 1a).

Drawing on the experience of wide-azimuth data from land and OBC, modeling work for diffracted multiples (Keggin et al., 2002), 2D illumination studies through the Messinian, and from limited towed-streamer MAZ examples like Varg (Resknes et al., 2002), it was decided to acquire a 500 km^2 dual-azimuth test in 2003. The uplift gained over the single-azimuth data was sufficient to justify the acquisition of the world's first six-azimuth survey in 2004—by repeating a legacy 650 km^2 survey five more times at 30° sail-line direction increments, in successive passes of the same towed-streamer recording configuration (Figure 1b).

Each azimuth sector was processed as a separate data set on its own 12.5 × 25 m grid, through a common flow—the flow applied to the existing (year 2000) E–W legacy data set. One additional step was required to match the phase and amplitude of the legacy azimuth to the five new azimuths. Each azimuth data set was prestack time migrated with the legacy time migration velocity field, and output onto a common E–W 25 × 25 m grid. Each data set then had dense, independent residual moveout (RMO) stacking fields

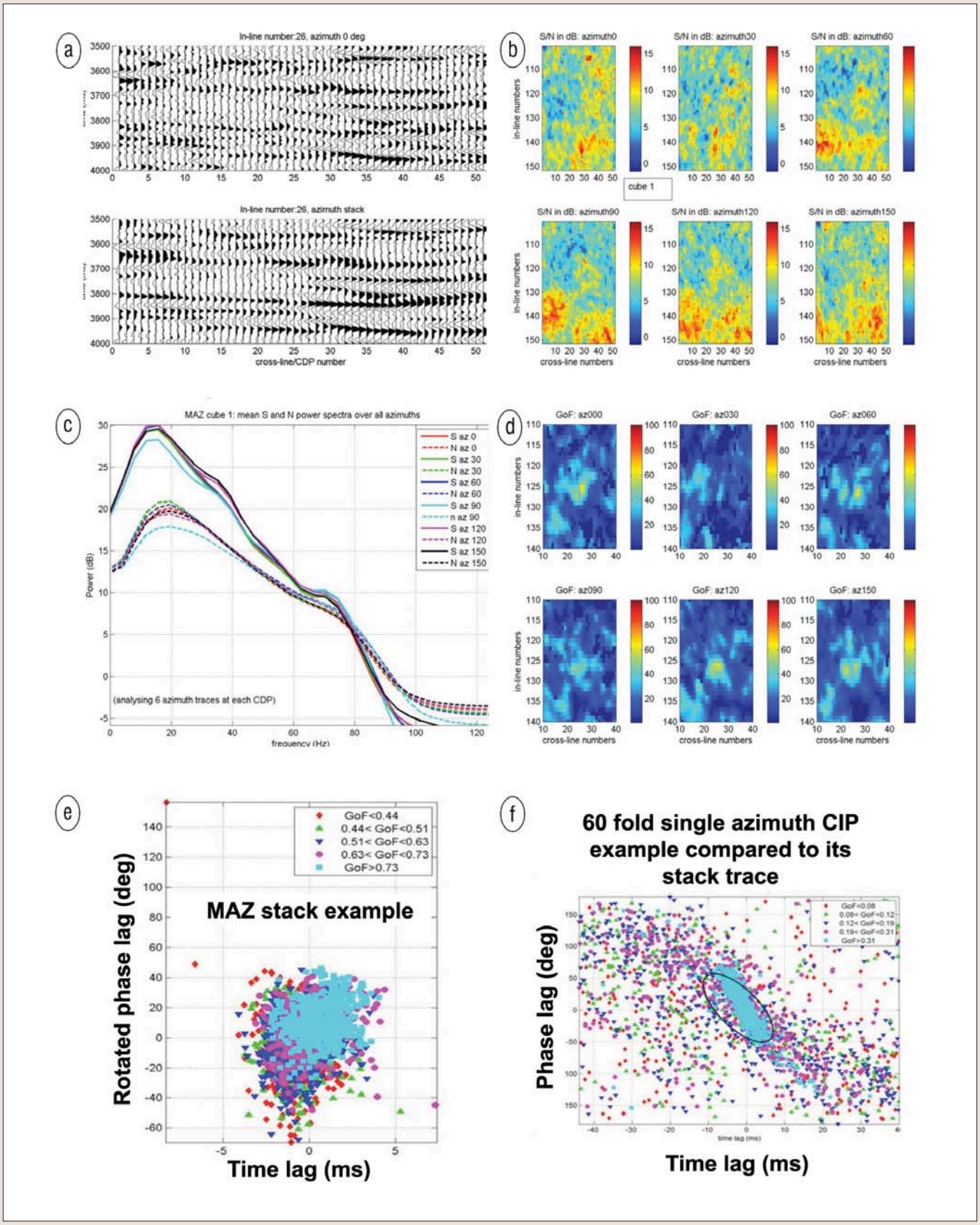

Figure 3. *S/N and focusing analysis of Raven MAZ data from a 50 × 50 CIP cube. (a) (top) Single-azimuth stack section; (bottom) much-improved MAZ section simply stacking the other five azimuths. (b) Map plots of a test cube for each azimuth, showing S/N variability over the same subsurface showing better data quality on some azimuths compared to others. Blue is poor, and red is good S/N. (c) Calculated signal and noise spectra for each azimuth stack; note the legacy azimuth 90° (cyan) is the poorest and requires a bulk scalar to match the other five azimuths. (d) Focusing analysis of each azimuth stack compared with a reference signal from the stack of all azimuths. The strong bull's-eye in the center indicates very good focusing in all apart from az30° in this example. (e) Time and phase lags are estimated at less than one sample for the azimuth stacks (after RMO). (f) Time and phase lags estimated before rotation to be in the tens of milliseconds range beneath the Messinian in a CIP gather.*

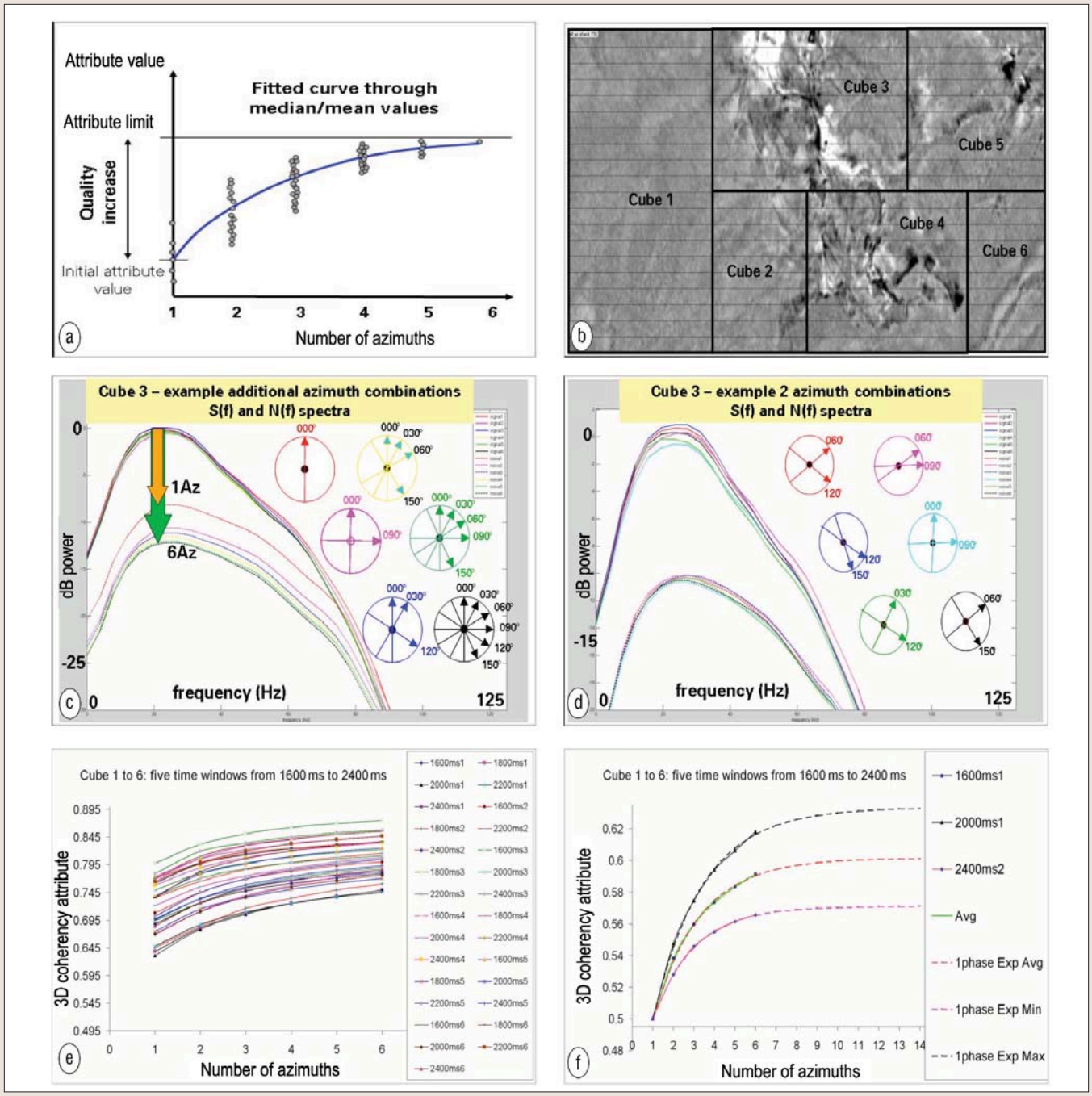

Figure 4. *Quantifying the incremental value of additional azimuths using quality curves. (a) The anatomy of a "diminishing returns" quality curve. Note the spread of quality values for a given number of azimuths and how this spread reduces with additional azimuths. (b) Time slice as 2 s showing the test data analyzed. Note the strong channel feature going from cube 3 to cube 4. (c) Six S/N spectra for increasing number of azimuthal combinations. (d) Illustrates the variation measured from six of the possible 15 dual-azimuth cases. (e) and (f) show quality curves and parametric fits for a 3D coherency attribute and are described in the text.*

calculated and applied.

Each of the six 3D azimuth sectors is different, containing different illumination and remnant noise below the Messinian layer. Figure 2 shows some prestack gathers from the MAZ data. There is a range of S/N ratios, variable image continuity, and imperfect image positioning despite being processed through an identical sequence. While some of these differences encapsulate the reason for acquiring MAZ data in the first place, that is, sampling noise trains differently, and recording different raypaths, other differences are due to difficulties in processing this data and the limitations of time imaging. Both of these reasons pose an obstacle to the best azimuth combination at all locations.

Further background to, and application of the multi-azimuth (MAZ) seismic technique to Raven Field is covered by Keggin et al. (2007). Rietveld et al. (2007) discuss MAZ processing and interpretation results, and Page et al. (2007) discuss MAZ acquisition and additional processing.

Part 1: Multi-azimuth (MAZ) analysis and quality. Let us consider a CIP location within the Raven MAZ data sets from what is considered to be a poor data area. Each azimuth CIP contains 60 fold with the migrated offset classes ranging from 350 to 6250 m in 100 m increments. On the 25 × 25 m output grid there will be six such subsurface CIPs—acquired at azimuth bearings 0°, 30°, 60°, 90°, 120°, and 150°

—all estimating the same subsurface reflectivity from different source to receiver azimuths and offsets.

Figure 2 shows how different these estimates of the same subsurface points are after identical processing and with azimuthal RMO applied. Indeed, if they were identical this would have been a very expensive and pointless experiment. Note that the signal and the noise character changes both with offset and azimuth.

To quantify the S/N, phase, timing, and spatial consistency of the data, methods similar to those described by Thomas et al. (1998) have been applied. One aim was to separate residual time shifts between the azimuths from those due to the bandwidth and phase of the data, and another was to determine how well focused the images were after migration. Figure 3 illustrates some of the findings from a 50 × 50 CIP cube, windowed from 3.5 to 4 s (the complex Messinian is at approximately 3 s). Figure 3a shows the clear improvement achieved for an example stack section from a single azimuth (top) and the same section with the other five azimuths stacked as well (bottom).

The different azimuth stacks show variable S/N ratios for the same subsurface (Figure 3b) with some azimuths having three times the estimated S/N ratio in one area compared to the same area in another azimuth. Below the Messinian, where the data set is being analyzed, the noise floor crosses the signal above 60 Hz—potentially allowing for significant resolution gain with the cleaner MAZ stack data (Figure 3c). The legacy data azimuth (cyan) is shown to be anomalous after migration on these spectra and requires an amplitude correction to match the other surveys. Each azimuth stack is very well focused spatially (Figure 3d) despite the use of time migration with a single smooth velocity field, and in the presence of a complex dipping water bottom. A rotated time and phase analysis (Figure 3e) of the RMO stacks shows them to be resolved to within 1 sample (4 ms) while the same analysis across offsets shows an order of magnitude greater errors in the CIP compared to its stack trace (Figure 3f).

In summary, the Raven 6MAZ combines successfully due to good temporal and spatial registration, and by having similar spectra (wavelets). This has been achieved by both similar acquisition and processing and the absence of strong anisotropy.

Part 2: How many azimuths are needed? This is a frequently asked and important question, not least because of the incremental cost of additional 3D marine surveys. Undoubtedly the answer is related to the complexity of the overburden—the size and strength of the distorting velocity lenses for example, and the resolution required at the target. For the current analysis we use the concept of quantitative "quality curves," (Figure 4a). The idea is to identify attributes from the stacked data that are reliable indicators of seismic quality and then to measure all possible combinations of azimuthal data sets. For six azimuths that means we can measure six mono-azimuth stacks, 15 dual-azimuth (DAZ) stacks, 20 tri-azimuth (3MAZ) stacks, 15 four-azimuth (4MAZ) stacks, six five-azimuth (5MAZ) stacks, and finally one six-azimuth (6MAZ) stack. This gives us a total of 63 combinations of the six azimuths (Figure 4a). Note the spread of quality points along the *y*-axis for each number of azimuths location on the *x*-axis. Different quality attributes produce different curve shapes.

Let us examine the S/N ratio we discussed for each individual azimuth earlier. Figure 4c shows the improving S/N quality for six of the 63 possible combinations; mono-azimuth 0°, dual-azimuth 0°+90°, 3MAZ 0°+30°+120°, 4MAZ 0°+30°+60°+90°, 5MAZ 0°+30°+60°+90°+150° and the 6MAZ. Note that the single azimuth 0° has an average S/N ratio=3.5, and is included in the dual-azimuth stack with an average S/N ratio=5.5. Note also that the signal level remains little changed but the noise floor is pushed down with additional azimuths by about 5 dB (orange to green arrow); the final 6MAZ average S/N ratio=8.0. Figure 4d illustrates the spread of S/N ratios from six of the 15 possible different dual-azimuth combinations. Once again the legacy data combinations are anomalous, but the overall result is similar for each combination (average S/N range is 5.5–6.1). For the quality curves we will calculate all possible combinations and plot the median quality value to represent each number of azimuths.

Figure 4e shows the quality curves for a 3D coherency attribute, calculated for all six spatial and five temporal cubes—30 analysis areas above the Messinian. The median curve through each area's 63 combinations (a total of 1890 quality calculations per attribute analyzed) is plotted and shows a clear trend toward diminishing returns. Figure 4f is based on the curves in 4e, but first they are bulk-shifted to start at the same value, 0.5. Parametric fitting (Equation 1) is shown by the dashed lines for the minimum, average, and maximum measured quality curves. These are then extrapolated beyond six azimuths.

A very good parametric curve fit ($R^2 \approx 0.999$) to the median attribute value of each combination is a nonlinear single phase exponential decay:

$$Q = A\,(1 - e^{(-B * N + C)}) \qquad (1)$$

where A represents the quality limit, N the number of azimuths, and B and C are related to the rate at which the additional azimuths add value and the potential value possible. This fit is partly chosen because the coherency value cannot exceed 1, which is useful for constraining the extrapolation beyond the number of azimuths available.

Assuming this model, it is possible to fit Equation 1 to any 3MAZ data sets and solve for A, B, and C. This has practical application because BP acquired two 3MAZ surveys in the Nile Delta at the end of 2006, and this approach could be used to describe the quality curve for these surveys and so predict the incremental value of additional azimuths should they be required, and also to determine the quality limit for that area.

For the Raven 6MAZ the model suggests that more than 90% of the maximum quality has been achieved, and that eight azimuths is the useful maximum with no discernable return after 10 azimuths (Figure 4f). The analysis also shows that quality always increases with additional azimuths for the best azimuth combinations (i.e., the best or median of the 4MAZ quality attribute is always better than the best or median for the 3MAZ case). However, an additional azimuth from a poor data area (or one not well matched or registered to the others) may decrease the quality of the multi-azimuth stack. The quality range for a fixed number of azimuths is thus a good indication of data quality and may indicate when to do additional processing or drop an azimuth from the combination. As discussed in part 1 of this paper, these curves reflect the case when the different azimuths are well registered and contain the same wavelet.

The coherency curve fitting terms show a reasonable stability for this part of the Nile Delta; the 20–30% variation that is measured is taken to represent changes from complex to simple geology (relative to the areas examined). For the mono-azimuth case, by assuming the quality limit A, it would then be possible to generate a quality curve using

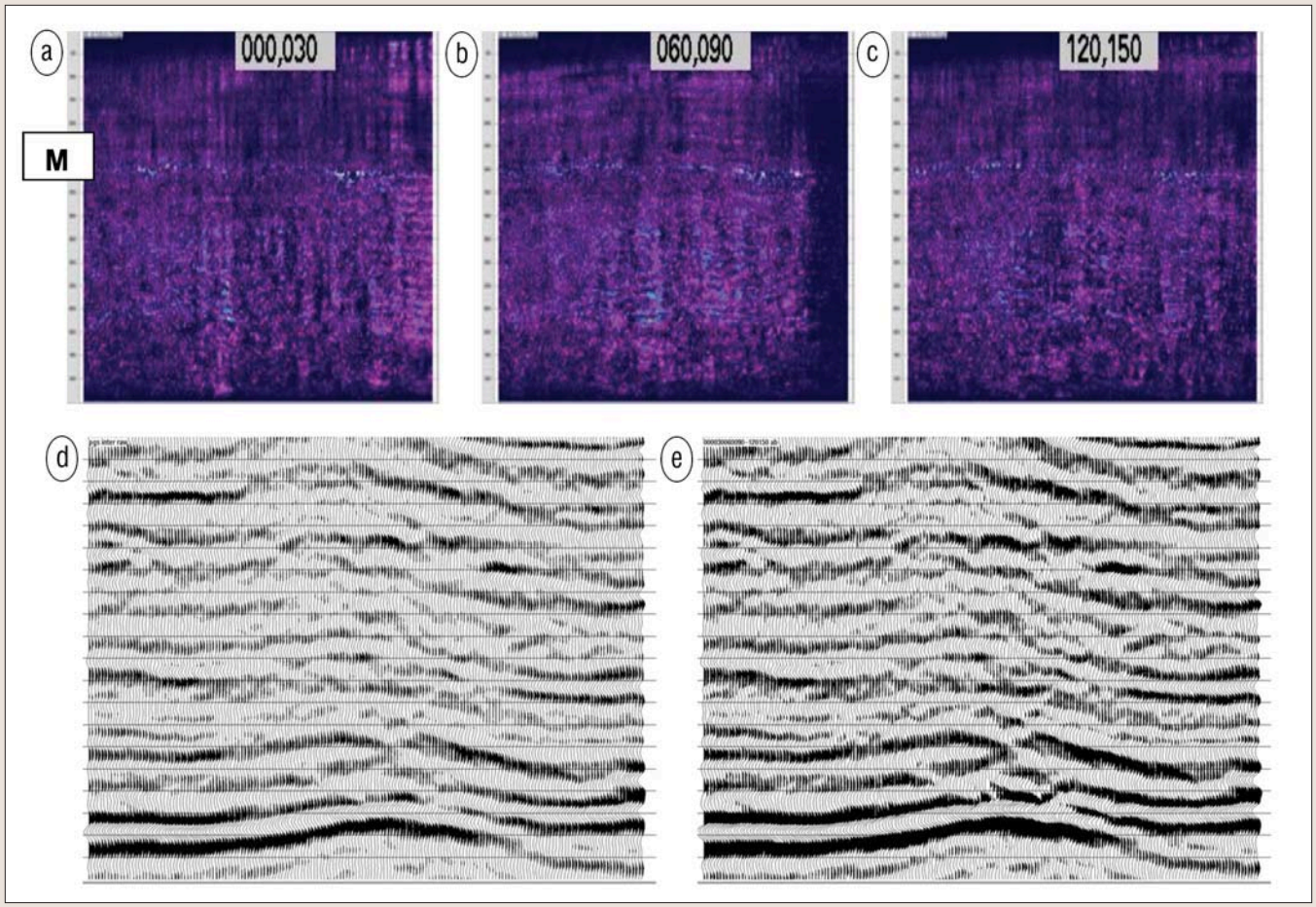

Figure 5. *Addback concept illustrated in 2D. (a) Example 1, Az0° and Az30° sail-line difference energy (instantaneous amplitude from 0 to 6 s) where M indicates the Messinian layer. (b) Example 2, Az60° and Az90° difference energy. (c) Example 3, Az120° and Az150° difference energy. (d) Zoomed section from the central area of the above differences: mean MAZ stack. (e) Mean MAZ stack with addback. These examples mostly show differences in illumination that, after filtering, can be used to weight the final MAZ stack and compensate for the conventional stack weighting down amplitude in areas with only partial illumination.*

representative *B* and *C* values for an area.

Work is under way to extend these initial findings to different MAZ surveys to determine if this model has widespread applicability.

Part 3: Optimized stacking tradeoff: Best image versus noise suppression. When illumination holes are a big problem, azimuthal diversity will help to more completely illuminate the subsurface. This means that some azimuths will be deficient in signal at a given location compared to others. One risk with combining noisy, nonilluminating azimuths/offsets and those azimuths/offsets with illumination is that the achieved illumination may be degraded or "stacked out." This is difficult to predict without having the azimuths for analysis. Averaging all subsurface illumination points may not be the best approach to maximize signal contribution. Conversely to the illumination case is the noise suppression case. Diffracted multiple and random noise are best attenuated by using all the recorded azimuthal diversity and high fold.

Thus a tradeoff exists between the suppression of global noise and the enhancement of partial local signal.

Conventional stack discussion. The common reflection point method (Mayne, 1962) calculates the mean amplitude across the offsets for each time sample to improve the S/N ratio. The robustness of this stack has been a fundamental part of the seismic toolbox since its inception, and still is the standard technique in spite of a plethora of other stacking algorithms, in line with the conclusions of White (1977).

While the conventional stack is very good at suppressing uncorrelated noise, there are limitations—for instance, the statistical mean is not robust to outlier noise.

Another problem for the mean estimate occurs when illumination varies within the common image point (CIP) with offset and/or azimuth, as discussed above. Consider the undershooting of a shallower seismic anomaly by long offsets. The mean amplitude over all offsets will result in the stacked amplitude strength being weaker than the case where the mean is limited to only the traces that contain signal. The question then becomes, "How can we obtain more accurate primary amplitudes in the partial absence of signal?"

Addback: 0 + 1 = 2. Consider a dual-azimuth case where one of the azimuths illuminates an event (value = 1) and the other does not (value = 0). The conventional stack will return half of the illumination (value = 0.5), ignoring for now the effects of noise. Thus the stack of all the parts (offsets and azimuths) may not be as good as the best of the parts from the illumination point of view.

Figure 5 illustrates the addback concept on the 6MAZ Raven data, aimed at weighting up the areas with partial illumination, so that 0 + 1 = 2. The approach adds the absolute value of the coherent signal in the difference volume between two azimuths back to the sum of the two azimuths, matching the stacked polarity. This way, all off-

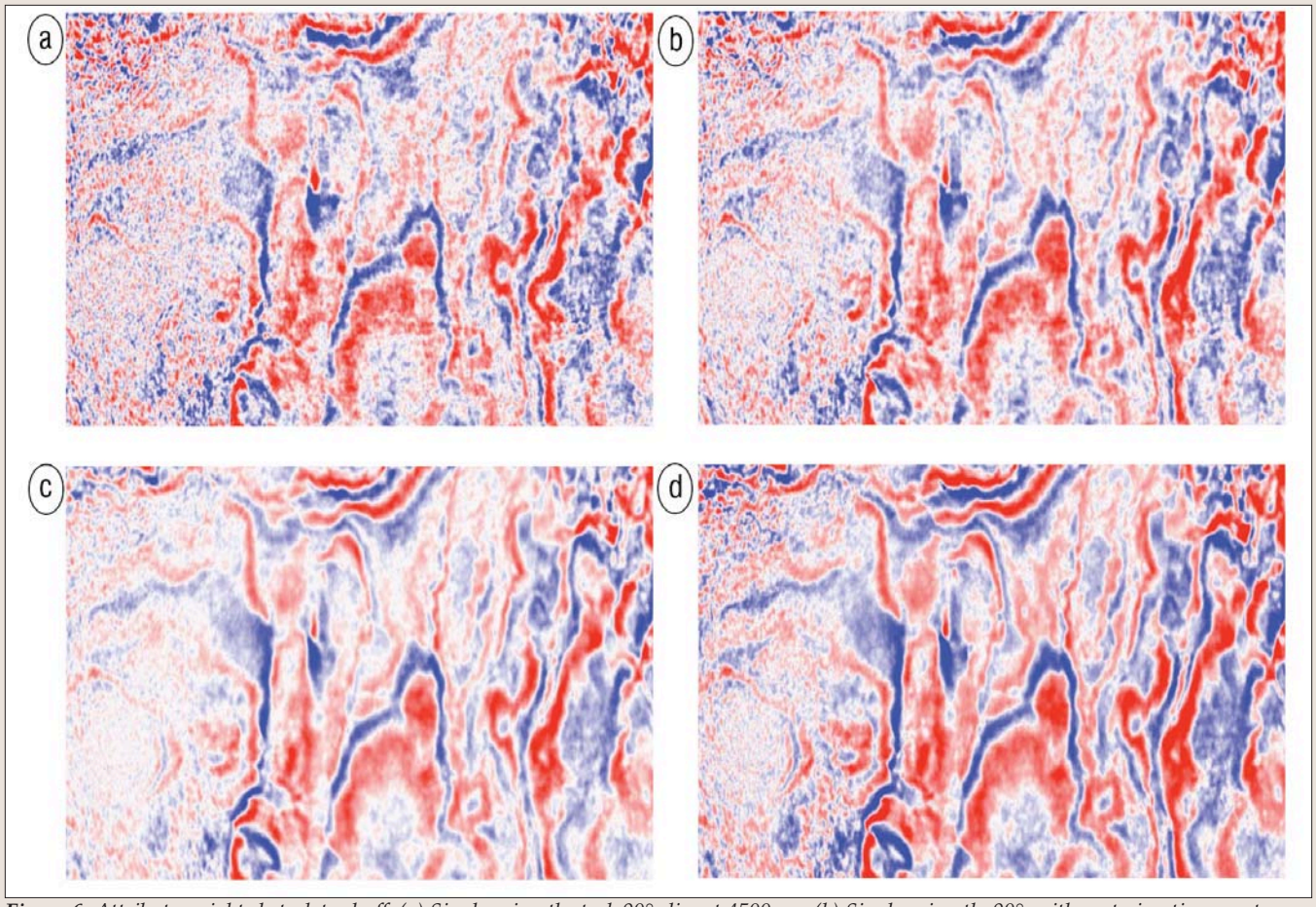

Figure 6. *Attribute weighted stack tradeoff. (a) Single azimuth stack 90° slice at 4500 ms. (b) Single azimuth, 90°, with postmigration event flattening and noise attenuation. (c) Simple 6MAZ stack of Figure 6b with the other five azimuths. (d) Amplitude-weighted 6MAZ stack showing subtle amplitude weighting benefits compared to 6c.*

set traces are used in the mono-azimuth stacks to help with S/N, and the difference energy is used to weight up the partial illumination. For more details see Manning et al. (2006) and Rietveld et al. (2007). For 6MAZ data the approach requires five addbacks to complete. Figures 5a–c show the poststack difference energy for three of the five steps—the instantaneous amplitude differences as described in Equation 2. The bright colors indicate areas where one azimuth has more energy than the other (and is assumed to be better illuminated). Note that the energy is strongest below the Messinian and the variable pattern of energy in each azimuth difference. This method, compared to a simple difference, is less sensitive to timing errors between the stacks and is calculated as follows:

$$D_{12} = [(\cos(IP_1) + \cos(IP_2)) / 2] * [IA_1 - IA_2] \qquad (2)$$

where D_{12} represents the difference between azimuth 1 and 2, IP_1 the instantaneous phase and IA_1 the instantaneous amplitude for azimuth 1. Figures 5d and 5e show a seismic 6MAZ example with and without addback.

The advantages of addback are that it is data driven and allows 3D filtering techniques to clean the difference data before addback. The main drawback is that it does not distinguish signal from noise by itself and so requires noise attenuation first; it also assumes that the data are well aligned and in phase, which may not be the case.

Weighted stacks. There are several available stack options other than taking the sample average as the estimate of subsurface amplitude, for example, diversity stacks, alpha-trim stacks, and power stacks. These, however, do not address the underlying tradeoff between noise suppression (stacking all the data) and illumination weighting (only stacking the parts with signal). In principle the optimum solution is to reject offsets and azimuths without signal and therefore lose a little on the random noise suppression side to help with signal amplitude levels.

Figure 6a shows a pre-Messinian time-slice through a single-azimuth stack volume after prestack time migration; 6b shows the uplift that can be achieved by additional prestack processing, primarily event flattening and offset amplitude balancing, and 6c is the result of stacking all six azimuths together with time-varying trim statics to account for residual timing differences. Figure 6d shows the additional uplift from a weighted stack method to address the tradeoff just discussed. The tradeoff has been managed by integer weighting schemes, rejecting poor data areas from the stack (weight = 0), and then possibly including other azimuths more than once, based on attribute measurements of the data quality.

The advantage of this is that it is data driven, and attempts to optimize the tradeoff between S/N attenuation and variable illumination preservation. A drawback is that it will require some parameterization and additional noise attenuation processing.

Mediancentre stack. Statistically, the Raven MAZ data set has the advantage of 6 × 60 estimates of the subsurface at a given image location. As mentioned earlier, the mean is

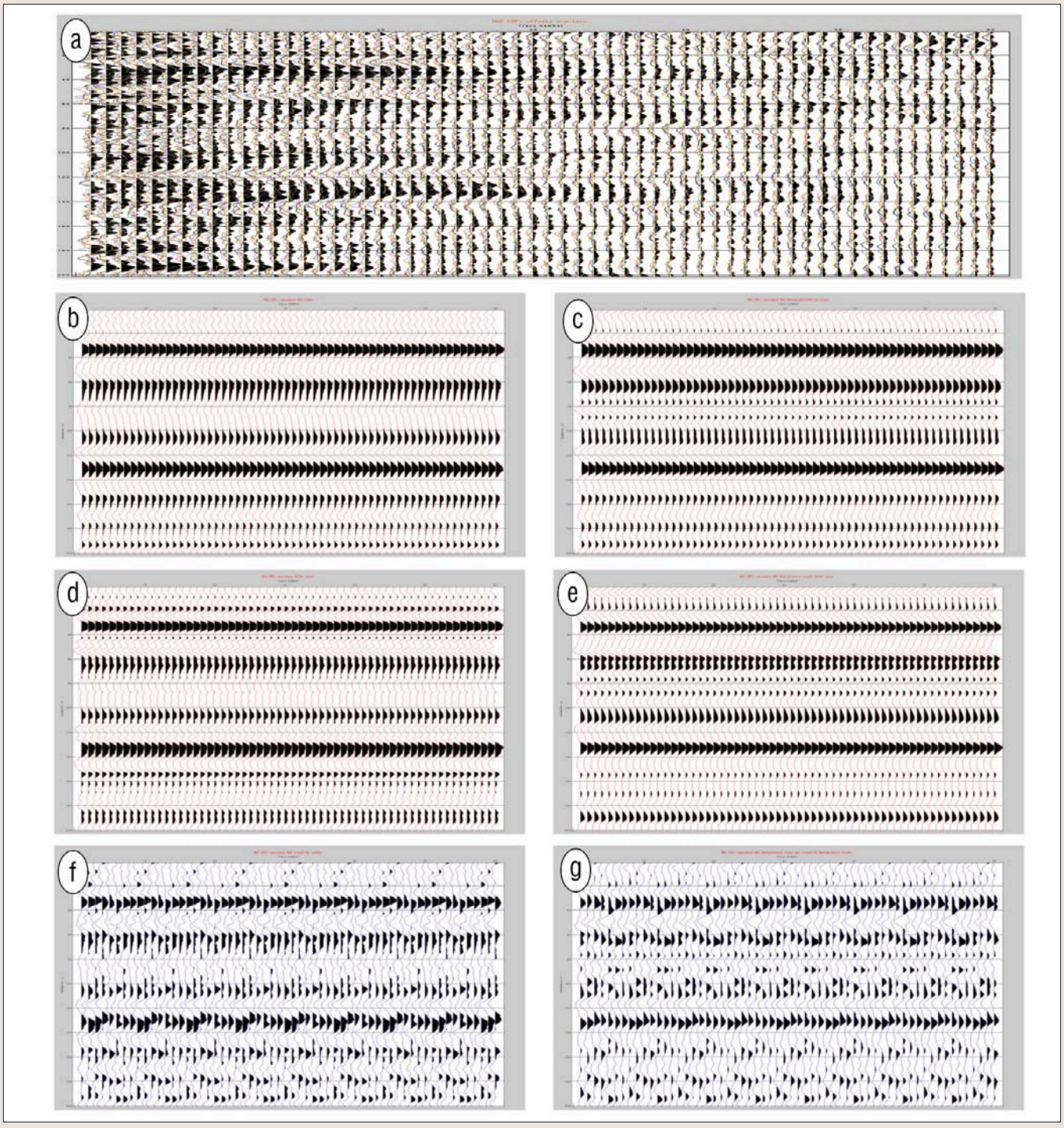

Figure 7. *Mediancentre stack. (a) A single 360-fold CIP zoom, all 60 offsets, with all six azimuths overlain. (b) Conventional stack of Figure 7a reproduced 60 times for display. (c) The mediancentre MAZ stack for all 360 traces in 7a repeated. (d) Conventional stack of azimuth 0°, repeated. (e) Mediancentre stack of azimuth 0°. (f) Sequential simple azimuth stacks, (6MAZ, Az1, Az2, Az3, Az4, Az5, Az6) repeating. (g) Sequential mediancentre azimuth stacks arranged as in 7f.*

not a robust estimate in the presence of outlier noise.

The median stack in *t-x* domain is more robust to outliers but does not result in a smooth output trace and so is not liked by interpreters. An alternative statistical approach is described by Bedall and Zimmerman (1979) and is a type of spatial median or mediancentre in the complex plane. This procedure corresponds to the minimization of the L1 norm and has a breakdown point of 50% just as the 1D median does—that is, at least half of the values passed to the algorithm must estimate signal.

Figure 7 shows some results from this approach and contrasts with the conventional mean stack. Figure 7a represents a zoomed CIP from a poor data area with 360 traces. Each azimuth is overlain in a different color to illustrate the variability in the subsurface measurements. The mean or stacked trace for all this data is shown in Figure 7b. Calculating the mediancentre of all 360 offset and azimuth traces (Figure 7c) shows less noise and more resolution compared to 7b. Figure 7d and 7e compare the mean and the mediancentre for a mono-azimuth stack, once more with significant improvements. Figure 7f and 7g show the resulting azimuth gathers for this location, repeated for display. The mean in

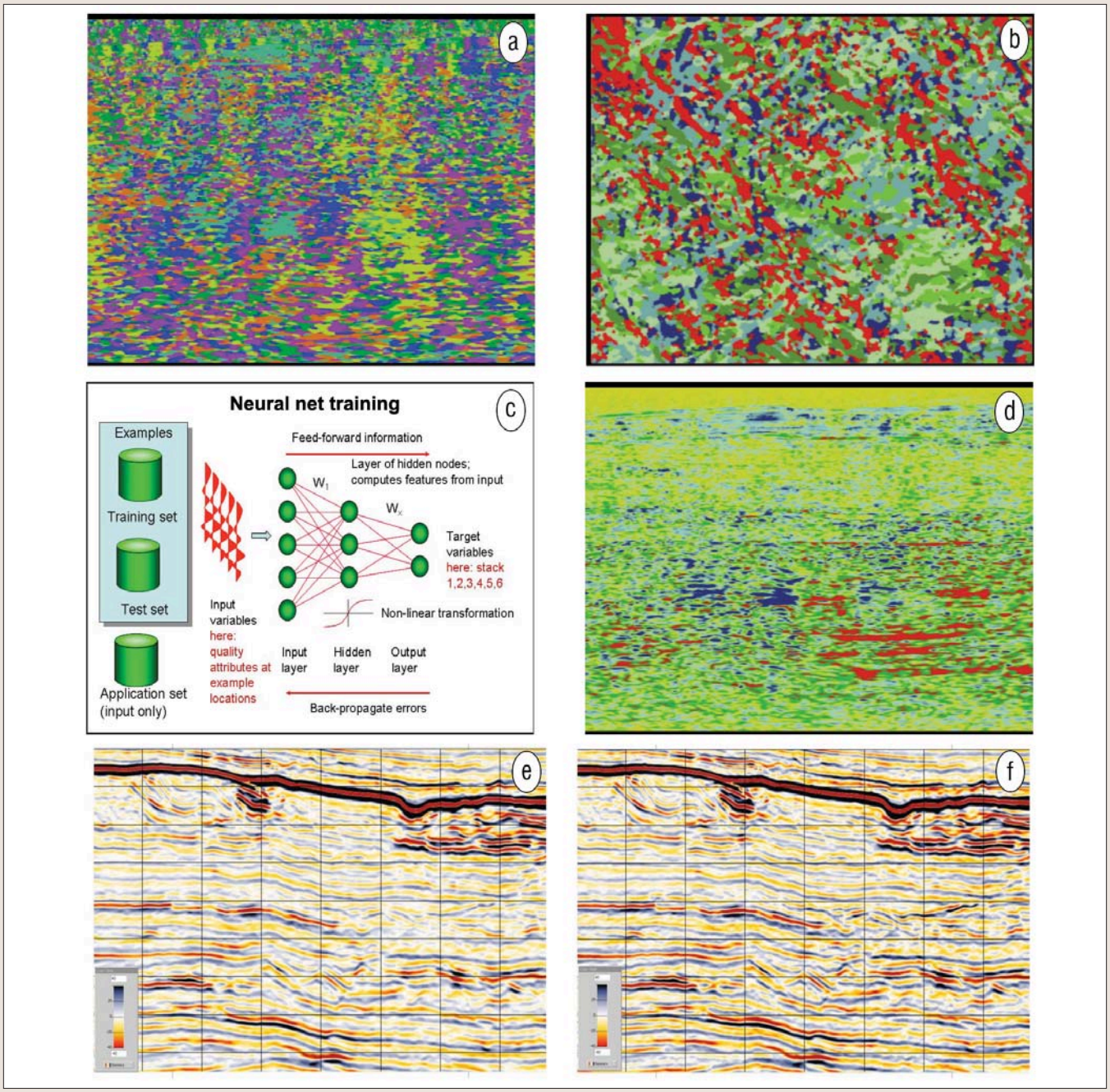

Figure 8. *Artificial neural network (ANN) weighted stack. (a) Vertical section through an MAZ stack made by selecting the best azimuth at each location, termed the winner cube (0–6 s). Each color represents a different azimuth. (b) Horizontal slice though the winner cube showing the spatial distribution of the high-graded azimuths, e.g., red=150°. (c) Schematic of the ANN used. (d) Vertical section for a single-azimuth stack showing the resulting ANN weights applied before MAZ stack. (e) Vertical section showing the dip-steered, median-filtered MAZ stack without weights. (f) ANN stack, to be compared with Figure 8e showing improved amplitude continuity.*

7f is noisier and lower in resolution than the mediancentre in 7g, which also highlights a residual azimuthal timing pattern more clearly than does the mean estimate.

Additional work on this approach suggests that weighting according to the "spread" of data in the complex plane (using the median absolute deviation from the mediancentre) has the potential to deliver further improvements.

An advantage of this technique is that it is a better estimate than the *t-x* average because it is robust to outliers. The drawback is that it is robust only if 50% of the data contain good estimates, as for any statistical technique, and it is more compute intensive than simple stack but this could be improved by a factor of 10 (Somorcik, 2006).

Artificial neural network (ANN) stacks. When an interpreter is given six different azimuthal images of the subsurface under a complex overburden, it is quickly evident that no one azimuth is best everywhere. The trained eye can evaluate subsets of one image that are preferable to another. If this observation can be posed in terms of quality attributes derived from the seismic, then an artificial neural network can be trained via a supervised learning approach to weight each azimuthal contribution based on the interpreter's winning picks.

The azimuthal data sets are analyzed automatically, after noise filtering and alignment, to select the best azimuth at each location and combine into what is termed a *winner cube*.

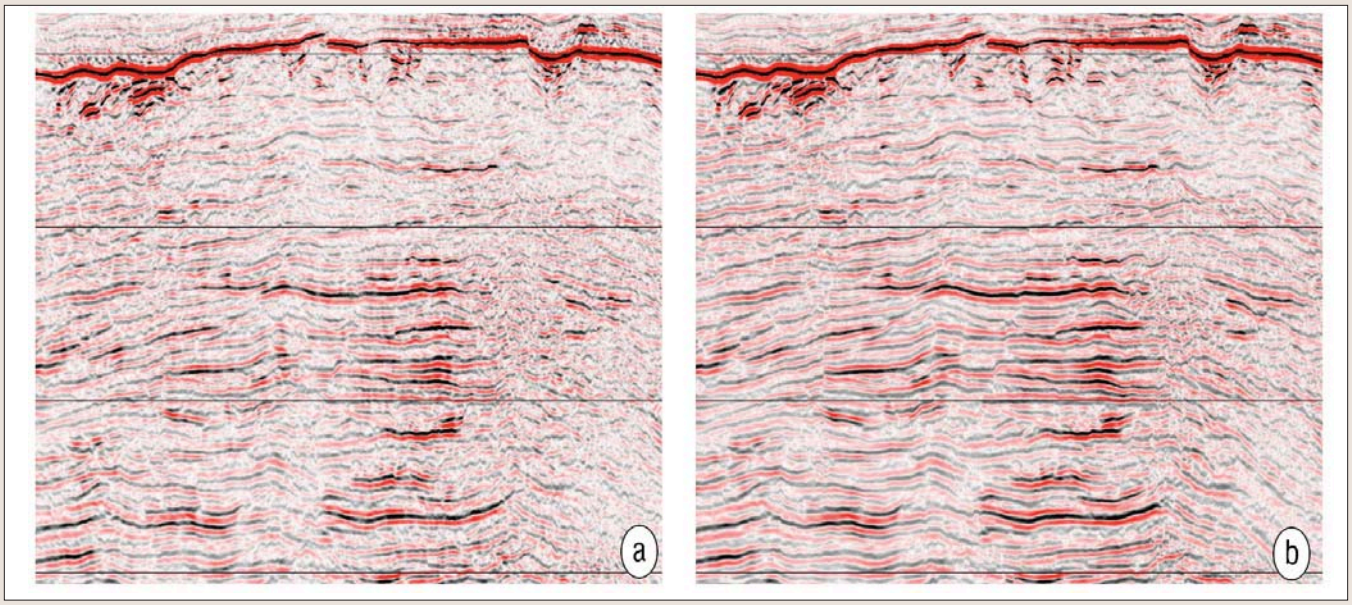

Figure 9. *Pre-Messinian data quality uplift example. (a) Mono-azimuth stack with flattening and offset amplitude compensation. (b) Result with the additional five azimuths and a weighted stack.*

This is used to limit the amount of data that the interpreter must review. Figures 8a and 8b show how the azimuths contribute to the winner cube. The interpreter can use this guide to manually and subjectively pick areas of good data that have been high-graded in the winner cube. The chosen locations are used to train the network (Figure 8c) and weight the six incoming azimuth stacks in a nonlinear fashion.

The weights can be reviewed and show conformance to the seismic (Figure 8d). The tradeoff between weighting and noise suppression is achieved by combining all the data, but with the best data weighted highest and the data with no signal weighted very low.

The advantage to this approach is that it can potentially learn directly from the interpreter and then calculate and apply weights to every sample in the 3D volume accordingly. The main drawback is that, as with all neural network solutions, the results can be difficult to learn from.

Conclusions. Multi-azimuth (MAZ) seismic data acquisition is designed to solve two data quality problems—poor S/N ratio and poor illumination (image quality). In our analysis of the six-azimuth data set over Raven in the Nile Delta, the significant improvements that have been reported for MAZ data (see Rietveld et al., 2007, and Keggin et al., 2007), can be understood in terms of quantitative S/N estimates, and timing and focusing measurements which reflect good (not perfect) spatial and temporal registration of the different azimuth volumes.

We have outlined a method to quantify the incremental value of each additional azimuth for the Raven 6MAZ. The parametric curve fitting shows that the quality curves are stable and may be used for extrapolation and prediction. The approach suggests that the quality limit has almost been reached with six azimuths at Raven, a development quality seismic data set.

Another conclusion from this analysis is that the number of azimuths is not the sole factor in the data improvements seen; rather, it is the azimuthal diversity—for example, not all of the dual-azimuth combinations are the same.

This work has also highlighted a challenge to optimally combining MAZ data and discussed the tradeoff that may exist between a conventional stack using all azimuths and all offsets and an optimized stack. Alternatives such as addback, weighting schemes, mediancentre stack, and supervised artificial neural network stacks were introduced to give the reader a flavor of different techniques for the optimized stacking combination. Figure 9a shows a mono-azimuth seismic section after full processing representing the best quality data currently possible from narrow-azimuth towed streamer data, while 9b is a weighted stack of all six azimuths.

In short, while the simple mean works very well, there are alternative techniques to conventional stack now available. In additional, these alternative stacking techniques may well have application to other single or multi-volume seismic data sets, e.g., 4D and 4-C data, or with survey merges.

Suggested reading. "Algorithm AS143: The mediancentre" by Bedall and Zimmermann (*Applied Statistics*, 1979). "Multi-azimuth 3D provides robust improvements in Nile Delta seismic imaging" by Keggin et al. (*First Break*, 2007). "Attenuation of multiple diffractions by multi-azimuth streamer acquisition" by Keggin et al. (EAGE 2002 *Expanded Abstracts*). "Multi-azimuth (MAZ) towed streamer data processing flow from the Nile Delta" by Manning et al. (*SEG 2006 Expanded Abstracts*). "Common reflection point horizontal data stacking techniques" by Mayne (GEOPHYSICS, 1962). "Towed streamer multi-azimuth processing and acquisition" by Page et al. (*First Break*, 2007). "How PGS created a new image for theVarg field" by Reksnes et al. (*First Break*, 2002). "Multi-azimuth towed streamer 3D seismic in the Nile Delta, Egypt—processing solutions" by Rietveld et al. (*First Break*, 2007). "Tests using spatial median" by Somorcik (*Austrian Journal of Statistics*, 2006). "Quantitative controls on 3D seismic processing for prestack attribute analysis" by Thomas et al. (*TLE*, 1998). "The performance of optimum stacking filters in suppressing uncorrelated noise" by White (*Geophysical Prospecting*, 1977). TLE

Acknowledgments: Roy White consulted on and provided code for the MAZ timing and focusing analysis and QC. Andrew Walden consulted on and provided code for the mediancentre stack. Paul de Groot and dGB carried out the neural network weighted stack. Thanks are due also to the other members of the collaboration team, Roald van Borselen, Adrian Burke, and Waleed Hussein. This work was carried out through a Technology Collaboration Agreement between BP and PGS. Thanks are due to BP, PGS, RWE Dea, and EGAS for permission to publish this work.

Corresponding author: Edward.Manning@uk.bp.com